ELSEVIER

www.elsevier.nl/locate/jorganchem

Journal of Organometallic Chemistry 598 (2000) 318–328

Journal of Organometallic Chemistry

Activation of a coordinated alkyne by electron transfer: crystal structures of [Pd{$PPh_2CH{=}C(Bu^t)NN{=}C(Bu^t)CH_2PPh_2$}{$C(CO_2Me){=}CH(CO_2Me)$}] and [Pd{$(Z,Z)PPh_2CH_2C(Bu^t){=}NN{=}C(Bu^t)CH_2PPh_2$}{$C(CO_2Me){\equiv}C(CO_2Me)$}]

M. Fernanda N.N. Carvalho [a,*], Adelino M. Galvão [a], Armando J.L. Pombeiro [a], Jan Čermák [b], S. Šabata [b], Pavel Vojtíšek [c], Jaroslav Podlaha [c]

[a] *Centro de Química Estrutural, Complexo I, Instituto Superior Técnico, Av. Rovisco Pais, P-1049-001 Lisbon, Portugal*
[b] *Institute of Chemical Process Fundamentals, CZ-16502 Prague 6-Suchdol, Czech Republic*
[c] *Department of Inorganic Chemistry, Universita Karlova, Hlavova 2030, CZ-12840 Prague, Czech Republic*

Received 25 November 1998; accepted 9 November 1999

Abstract

A new zerovalent complex [Pd{$PPh_2CH_2C(Bu^t){=}NN{=}C(Bu^t)CH_2PPh_2$}{$C(CO_2Me){\equiv}C(CO_2Me)$}] (**1**) was prepared and its crystal structure was determined by X-ray diffraction analysis, which shows it crystallises in the $C2/C$ monoclinic space group with $a = 10.940(1)$ Å, $b = 22.086(1)$ Å, $c = 19.042(2)$ Å and $\beta = 92.692(9)°$. The azine diphosphine ligand chelates the metal in a (Z,Z) configuration with a P–Pd–P bite angle of 114.63(4)°. The alkyne carbon atoms lie essentially in the P–Pd–P plane. The electrochemical reduction of **1** promoted the conversion of the alkyne ligand to a vinyl species, and of the azine diphosphine to *ene*-hydrazone diphosphine, with formation of [Pd{$PPh_2CH{=}C(Bu^t)NN{=}C(Bu^t)CH_2PPh_2$}{$C(CO_2Me){=}CH(CO_2Me)$}] (**2**). X-ray diffraction analysis of complex **2** shows it crystallises in the triclinic space group $P\bar{1}$ with $a = 11.302(1)$ Å, $b = 12.528(1)$ Å, $c = 16.028(2)$ Å, $\alpha = 107.64(2)°$, $\beta = 92.27(1)°$ and $\gamma = 111.79(2)°$. It displays a square-planar geometry with the two phosphorus atoms in *trans* position. Extended Hückel MO calculations were performed in order to elucidate the redox process.

Keywords: Electron transfer; Zerovalent complexes; Redox process

1. Introduction

The azine diphosphine, Z,Z-$Ph_2PCH_2C(Bu^t){=}N{-}N{=}C(Bu^t)CH_2PPh_2$ (Z,Z-P⌒P), was reported [1] to act as a bridging ligand at palladium and platinum complexes of general formula [{$(MX_2)(\mu$-Z,Z-P⌒P)}$_n$] ($n = 2$, Pd or $n = 6$, Pt; X = Cl [2] or 1/2 alkyne [3]). However, it acts as a chelating ligand for most of the transition metals forming mononuclear compounds by isomerisation to the (E, Z) form. In some low-oxidation-state metal sites, e.g. Au(I), Ag(I) or Cu(I), the Z,Z-P⌒P form is kept upon coordination [4].

The electronic and coordinative versatility of the azine diphosphine ligand makes it a convenient ligand for most of the transition metals, since it can act as a two-, four- or six-electron donor and occupy one, two or three coordination positions. The possibility of hapticity change is an important feature in the activation of organic substrates through coordination to metal sites.

Here we describe the reaction of the azine diphosphine (Z,Z-P⌒P) with a palladium(0) complex leading to the isolation and characterisation of a zerovalent complex in which the ligand displays the (Z,Z) configu-

* Corresponding author. Tel.: +351-846-237; fax: +351-846-4455.
E-mail address: pombeiro@alfa.ist.utl.pt (A.J.L. Pombeiro)

0022-328X/00/$ - see front matter
PII: S0022-328X(99)00730-5

ration. This result suggests that the (*Z*,*Z*) configuration is more common than thought previously.

The redox properties of **1** were studied by cyclic voltammetry and controlled potential electrolysis within our interest in the study of the electrochemical properties of coordination compounds.

For comparative purposes, the free azine diphosphine and the dimethylacetylene dicarboxylate were also studied.

2. Results and discussion

The reaction of $[Pd_2(DBA)_3]$ (DBA = dibenzylideneacetone) with the azine diphosphine (*Z*,*Z*-P⌒P) (Scheme 1), in aromatic solvents or THF leads to a mixture of three different compounds according to the phosphorus NMR spectrum (a singlet at 36.9 ppm, two other singlets at 26.9 and 31.4 ppm, and a nine-line pattern centred at 13 ppm). The appearance of the spectrum does not change on treatment of the mixture with phenylacetylene, propadiene, *tert*-butyl isocyanide, or carbon monoxide. However, upon addition of a stoichiometric amount of dimethylacetylene dicarboxylate, a new compound displaying a singlet at 36.0 ppm in the $^{31}P\{^1H\}$-NMR spectrum is formed.

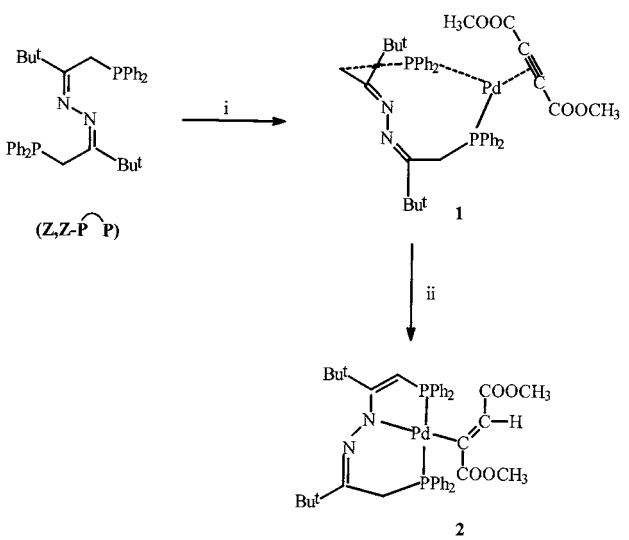

Scheme 1. Reagents and conditions: (i) $Pd_2(DBA)_3$ in toluene, then DMAD; (ii) controlled potential reduction at $E_p^{red} = -2.2$ V.

Table 1
Bond lengths (Å) for complex **1** [a]

Pd–C(4)	2.060(3)
Pd–P(1)	2.3229(8)
P(1)–C(31)	1.830(3)
P(1)–C(21)	1.841(3)
P(1)–C(1)	1.866(3)
C(1)–C(2)	1.504(5)
N(3)–C(2)	1.280(4)
N(3)–N(3) # 1	1.409(5)
O(6)–C(5)	1.317(5)
O(6)–C(7)	1.430(5)
C(2)–C(22)	1.533(5)
C(4)–C(4) # 1	1.258(7)
C(4)–C(5)	1.451(5)
C(5)–O(7)	1.189(5)

[a] Symmetry transformations used to generate equivalent atoms: # 1, $-x$, y, $-z+1/2$; # 2, $-x+1$, y, $-z+1/2$.

In the ^1H- and ^{13}C-NMR spectra, *tert*-butyl carbon atoms and protons are equivalent as well as the carbons and protons of ester groups. Methylene carbon atoms next to phosphorus appear as doublets but coordinated alkyne carbon atoms appear as a signal split into a doublet of doublets due to interaction with *trans*- and *cis*-phosphorus atoms. Methylene protons are not equivalent with relatively large differences in chemical shifts and are coupled only to the neighbouring phosphorus atoms, forming thereby two doublets of doublets. The corresponding methylene proton signal in the gold(I) analogue was found [4] to be a multiplet. We ascribed the different appearance of this signal in our spectrum to a bite angle smaller than in the gold complex and therefore lower coupling constant (< 1 Hz as shown by NMR spectrum simulation) between the phosphorus atoms.

Suitable crystals for X-ray analysis were grown from benzene–pentane as a benzene solvate.

2.1. Crystal structure of $[Pd\{PPh_2CH_2C(Bu^t)=NN=C(Bu^t)CH_2PPh_2\}\{C(CO_2Me)\equiv C(CO_2Me)\}]$

The complex displays a pseudotrigonal planar coordination sphere with the alkyne and diphosphine ligands oriented to give an overall C_2 symmetry for the molecule. The twofold axis is coincident with the crystallographic binary axis as a consequence of the special position of the heavy atom. The alkyne coordinates the metal as a η^2 ligand and the C–C bond is at the (P, Pd, P) plane (average deviation 0.02 Å). The geometry of the phosphorus atoms is tetrahedral and the Pd–P and P–C bonds lengths (see Table 1) are within the usual range [5,6]. The bite angle of the diphosphine is 114.63(4)° and the N–C double bonds are planar (the average deviation of the atoms C(1), C(2), C(22), N(3), is 0.06 Å) and oriented nearly perpendicular (87.00(8)°) to the coordination plane.

The molecule co-crystallises in a 1:1 ratio with discrete molecules of benzene. Selected bond lengths and angles are listed in Tables 1 and 2. Fig. 1 displays a view of the structure of complex with the atom numbering scheme.

Although nine-member rings are generally rare, they are often found [4] in systems with the azine diphosphine (*Z*,*Z*-P⌒P) ligand. The conformation of this ring

Table 2
Bond angles (°) for complex **1** [a]

C(4) # 1–Pd–C(4)	35.6(2)
C(4) # 1–Pd–P(1)	140.42(10)
C(4)–Pd–P(1)	104.93(10)
P(1)–Pd–P(1) # 1	114.63(4)
C(4) # 1–Pd–N(3)	158.73(11)
C(4)–Pd–N(3)	160.47(10)
P(1)–Pd–N(3)	59.44(5)
P(1) # 1–Pd–N(3)	56.33(5)
C(31)–P(1)–C(21)	101.6(2)
C(31)–P(1)–C(1)	104.2(2)
C(21)–P(1)–C(1)	99.3(2)
C(31)–P(1)–Pd	111.42(12)
C(21)–P(1)–Pd	112.45(11)
C(1)–P(1)–Pd	124.98(11)
C(2)–C(1)–P(1)	115.8(2)
C(2)–N(3)–N(3) # 1	114.4(3)
C(2)–N(3)–Pd	77.1(2)
N(3) # 1–N(3)–Pd	79.78(4)
C(5)–O(6)–C(7)	116.0(4)
N(3)–C(2)–C(1)	122.0(3)
N(3)–C(2)–C(22)	117.8(3)
C(1)–C(2)–C(22)	120.1(3)
C(4) # 1–C(4)–C(5)	145.9(2)
C(4) # 1–C(4)–Pd	72.22(10)
C(5)–C(4)–Pd	141.8(3)
O(7)–C(5)–O(6)	123.6(4)
O(7)–C(5)–C(4)	124.1(4)
O(6)–C(5)–C(4)	112.4(3)

[a] Symmetry transformations used to generate equivalent atoms: # 1, $-x$, y, $-z+1/2$; # 2, $-x+1$, y, $-z+1/2$.

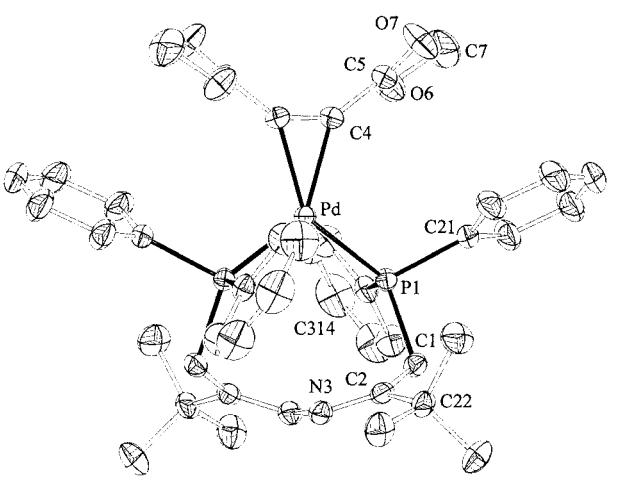

Fig. 1. Molecular structure of complex **1** displaying atom labelling scheme, ellipsoids drawn at 25% probability.

is strongly determined by the geometry of the two conjugated double bonds, which are both in the (*Z*)-configuration as confirmed by the torsion angle value (N, N, C, C = 7.4(4)°). In complex **1** the N–N bond distance (1.409(5) Å) is within the expected value for two sp^2 nitrogen atoms connected by a single bond (average value: 1.401 Å. [5,6]) and this bond is nearly perpendicular to the plane containing palladium and the atoms directly bound to it, due to the (*Z*,*Z*) configuration of both double bonds mentioned above. No bonding contacts exist between palladium and the nitrogen atoms (Pd–N(3) = 3.971(3) Å).

The palladium atom is localised at the special position 2, which makes the *tert*-butyl, phenyl and methoxy carbonyl groups occupy alternate positions towards the ring plane.

At the alkyne ligand the bond distance (C–C = 1.258(7) Å) is longer than that expected for a typical triple bond (1.20 Å) and the angle C(5)–C(4)–C(4) = 145.9(2)° is considerably bent, this being consistent with a decrease in the C–C bond order. The C–C=C–C moiety is nearly planar (7°).

2.2. Electrochemical studies

The palladium(0) complex [Pd{C(CO_2Me)≡C(CO_2Me)}(μ-*Z*,*Z*-P⌒P)] (**1**) displays by cyclic voltammetry, at a Pt wire electrode, in 0.2 M [NBu_4][BF_4]–THF, at scan rates lower than 200 mV s^{-1}, one irreversible cathodic wave at $E_p^{red} = -2.2$ V. However, at higher scan rates some degree of reversibility is observed, which increases with the scan rate. No original anodic process is detected. Upon reduction, on the reverse scan, one irreversible anodic wave is observed at $E_p^{ox} =$ 0.5 V. This behaviour is in agreement with the formation of a new species upon reduction, which is oxidised at that anodic wave (Fig. 2).

To have an insight into the cathodic process, we performed a controlled potential electrolysis in a THF solution of **1**, at the potential of its cathodic wave, using as working electrode a platinum gauze. After one electron per molecule was transferred, the work up of the electrolyte resulted in the isolation of *trans*-[Pd{PPh_2CH=C(Bu^t)NN=C(Bu^t)CH_2PPh_2}{C(CO_2Me)=CH(CO_2Me)}] (**2**) (for its full characterisation see below), as an orange crystalline solid (Scheme 1). The ^{31}P-NMR of the solution measured immediately after electrolysis confirms that no other product formed.

The study by cyclic voltammetry of complex **2** shows it displays one irreversible anodic and one reversible cathodic process, which occur at $E_p^{ox} = 0.5$ V and $E_{1/2}^{red} = -2.03$ V, respectively. The value measured for the anodic process agrees with that observed on the reverse anodic scan performed on the solution of complex **1**.

In order to gather information on the site where reduction occurs on complex **1**, we also studied by cyclic voltammetry the behaviour of the azine diphosphine (*Z*,*Z*-P⌒P) and the dimethylacetylene dicarboxylate. The former was found to oxidise at $E_p^{ox} = 1.02$ V (in CH_3CN) but no cathodic wave was detected, whereas the latter compound is reduced at $E_p^{red} =$ −1.90 V (in THF) and the cyclic voltammogram displays,

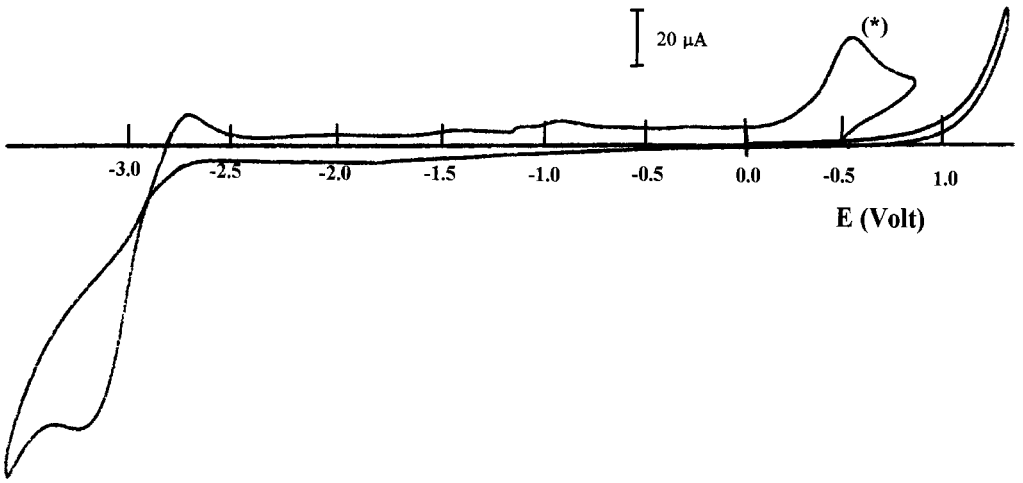

Fig. 2. Cyclic voltammogram of complex **1**, in 0.2 M $[NBu_4][BF_4]$–THF. Scan rate 200 mV s^{-1}. Potentials quoted versus SCE. (*) Anodic wave generated by reduction.

on the reverse anodic scan, following reduction, one oxidation wave at $E_{1/2}^{ox} = 0.16$ V; no original anodic wave was observed for the acetylene. These observations suggest that the reduction process of complex **1** is formally localised at the coordinated alkyne. As a result, a highly unstable intermediate (conceivably of the type of a) would be formed in which proton transfer from the CH_2 group of the azine diphosphine to the carbonion moiety would generate the vinyl ligand. At related complexes, the base deprotonation of the CH_2 group of the five-member ring of the *tert*-dentate azine diphosphine, with azine to *ene*-hydrazone conversion, was reported by Shaw and co-workers [3].

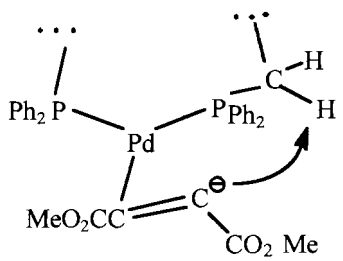

(a)

An alternative route, which cannot be completely ruled out, to explain the electrochemical behaviour observed, would involve the reduction of one of the imine groups of the azine backbone. Such a process would induce stereochemical changes at the azine diphosphine ligand and possibly hydrogen migration to the metal affording a hydride-type complex or a direct attack [7] of the methylene group to the C–C multiple bond. The hydride intermediate could then undergo alkyne insertion to give the final product. In the absence of any observable reduction process at the free azine diphosphine ligand, we favour the former process for which the initial electron input occurs at the alkyne ligand.

In addition to the alkyne to vinyl conversion, induced by electrochemical reduction, the formal oxidation of Pd(0) to Pd(II) also occurs.

A pronounced geometric rearrangement accompanies the alkyne to vinyl conversion, since at complex **2** (see below) the vinyl ligand occupies a plane perpendicular to the metal coordination plane. Such a geometrical change brings one of the nitrogen atoms close enough to the metal to interact (see below) and is expected to enhance the palladium contribution to the HOMO, thus being a driving force to the oxidation of the metal.

This rationalisation is corroborated by some theoretical calculations by the extended Hückel method (see below).

Complex **2** was characterised by IR, ^{1}H-, ^{31}P{^{1}H}- and ^{13}C-NMR spectroscopic techniques, and FAB MS and the structure confirmed by X-ray diffraction analysis.

In the IR spectrum of **2** no separate bands attributable to $\nu_{C=C}$ or $\nu_{C=N}$ are clearly observed. However, in the stretching region of the carbonyl of the ester groups, a band is observed at 1700 cm^{-1}, a value considerably lower than that known ($\nu_{CO} = 1800$ cm^{-1}) for the complex **1** precursor. This behaviour suggests the coupling of the $\nu_{C=N}$ and $\nu_{C=O}$ IR bands, which then occur at intermediate values as observed before [8].

The ^{31}P{^{1}H}-NMR spectrum consists of an AB spin system ($^2J(PP) = 361$ Hz) observed at δ 25.5 and 44.8 ppm, relative to H_3PO_4, for the resonances of the two phosphorous atoms of the azine diphosphine ligand. The chemical shifts are comparable with those reported for the related complexes *trans*-$[Pd\{PPh_2CH{=}C(Bu^t)NN{=}C(Bu^t)CH_2PPh_2\}X]$ (X = Cl, Br or Me) [3], and although the coupling constant is considerably lower than those observed for the latter compounds (457, 459 or 409 Hz for X = Cl, Br or Me, respectively), it is well above the values (ca. 40 Hz) [9]

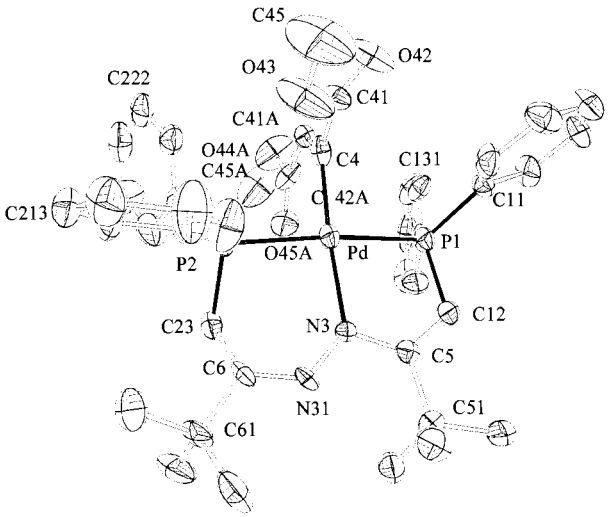

Fig. 3. Molecular structure of complex **2** displaying atoms labelling scheme.

Table 3
Selected bond lengths (Å) for complex **2**

Pd(1)–C(4)	2.00(2)
Pd(1)–N(3)	2.087(11)
Pd(1)–P(1)	2.257(4)
Pd(1)–P(2)	2.288(4)
P(1)–C(12)	1.754(14)
P(1)–C(11)	1.817(13)
P(1)–C(13)	1.82(2)
P(2)–C(21)	1.783(13)
P(2)–C(22)	1.81(2)
P(2)–C(23)	1.820(14)
N(3)–C(5)	1.38(2)
N(3)–N(31)	1.388(14)
C(4)–C(41A)	1.31(2)
C(4)–C(41)	1.48(2)
C(12)–C(5)	1.36(2)
C(6)–N(31)	1.31(2)
C(6)–C(23)	1.49(2)
C(6)–C(61)	1.55(2)
C(51)–C(5)	1.57(2)
O(42)–C(41)	1.19(2)
C(41A)–C(42A)	1.44(2)
C(41)–O(43)	1.31(2)
O(43)–C(45)	1.45(2)
O(43A)–C(42A)	1.20(2)
O(44A)–C(42A)	1.34(2)
O(44A)–C(45A)	1.41(2)

that have been reported for the related complexes with the *cis* geometry.

In the ^{1}H-NMR spectrum, the doublet of doublets ($^2J(PH) = 5.5$, $^4J(PH) = 1.5$ Hz) observed at δ 4.09 ppm is attributed to the C–H resonance of the enamine moiety of the diphosphine ligand, since these values are within the expected ranges [3]. The resonance of the methylene protons is observed as a multiplet at δ 2.97–3.06 ppm. The definitive assignment of these signals as well as the resonance of the vinyl CH proton (δ 6.04 ppm, dd; $^4J(PH) = 2.0$, $^4J(PH) = 0.5$ Hz), was accomplished on the basis of the COSY(H,C) correlation.

In the ^{13}C-NMR spectrum, the resonances corresponding to the CO carbon atoms (δ 186.6 and 189.4 ppm) of the ester groups are within the expected range. The resonances of the enamine (–C=C–N–) and imine (–N=C–) carbons occur at δ 167.3 and 174.3 ppm, respectively. At the vinyl ligand, the signal for the resonance of the coordinated carbon atom is observed at δ 145.3 ppm, while that of the =C–H carbon atom, it occurs at 129.0 ppm. Moreover, the doublet ($J(PC) =$ 54.9 Hz) observed at δ 72.3 ppm is assigned to the carbon atom of the *ene*-hydrazone of the diphosphine ligand. The COSY(C,H) correlation confirms this assignment.

The FAB MS spectrum clearly displays the molecular ion (m/z 815 [M + 2]), that upon fragmentation loses the vinyl ligand.

2.3. Crystal structure of *trans*-[Pd{$PPh_2CH=C(Bu^t)NN=C(Bu^t)CH_2PPh_2$}{$C(CO_2Me)=CH(CO_2Me)$}] (**2**)

The complex displays a square-planar geometry with the two phosphorus atoms of the diphosphine ligand in *trans* position to each other, as shown in Fig. 3. The relevant bond lengths and geometrical parameters are summarised in Tables 3 and 4, respectively. The palladium, nitrogen and vinyl carbon atoms lie 0.05 Å below the average plane containing the metal centre and the four coordinated atoms while the two phosphorus atoms lie 0.08 Å above it. The plane containing the vinyl ligand is almost perpendicular to the (Pd, C, P, P, N) coordination plane and bisects the azine–diphosphine ligand at the N(3) atom.

The atoms of the two cycles of the azine-diphosphine ligand display considerably different behaviour: the atoms in the five member ring are all below the (Pd, C, P, P, N) plane, as observed for the unbound nitrogen atom at the six member ring; at this ring the two carbon atoms are significantly above that plane, e.g. C(23) is 1 Å above it.

The ester group bound to the uncoordinated carbon of the vinyl is coplanar with C=C–Pd, while the other ester group makes an angle of 53° with it. Both the ester groups are planar with typical bond lengths and angles.

A projection of the position of the carbon atoms bound to the phosphorus atoms in a plane perpendicular to the P–Pd–P direction shows that the two halves of the diphosphine have alternate conformations.

The Pd–P and P–C bond lengths are within the normal range but the Pd–P(1) and P(1)–C(12) are slightly shorter (0.03 and 0.06 Å, respectively) than the Pd–P(2) and P(2)–C(23) bond lengths (Table 3).

Excluding the C(23)–C(6) bond length, which is clearly within the range commonly assigned to a single bond (1.49 Å), all the C–C, C–N or N–N bond lengths in the azine–diphosphine ligand display values between single- and double-bond character (1.31–1.39 Å). This feature is possibly a consequence of a considerable electron delocalisation through the P–N–P frame. The Pd–N distance of 2.09 Å is within the expected range [6] for palladium complexes with *tert*-dentated ligands, although stretched to the longer side of this range.

The C(4)–C(41) Å bond length (1.31 Å) at the vinyl ligand is longer than a typical C–C double bond, this pointing to a π-back donation effect from the filled metal d_{xz} orbital to the π* orbital of the ligand. This feature is reinforced by the perpendicular position of the vinyl ligand to the coordination plane (see Section 2.4).

2.4. MO calculations

The alkyne to vinyl conversion is accompanied by a major geometrical change at the ligand, which brings it from in-plane to perpendicular-to-coordination plane. This rearrangement increases the contribution of the metal to the HOMO and possibly is the driving force for the oxidation of the metal site.

Table 4
Selected bond angles (°) for complex **2**

C(4)–Pd(1)–N(3)	175.3(5)
C(4)–Pd(1)–P(1)	91.7(4)
N(3)–Pd(1)–P(1)	83.6(3)
C(4)–Pd(1)–P(2)	92.0(4)
N(3)–Pd(1)–P(2)	92.7(3)
P(1)–Pd(1)–P(2)	172.2(2)
C(5)–N(3)–N(31)	111.8(11)
C(5)–N(3)–Pd(1)	116.8(9)
N(31)–N(3)–Pd(1)	129.5(8)
C(41A)–C(4)–C(41)	115(2)
C(41A)–C(4)–Pd(1)	127.5(13)
C(41)–C(4)–Pd(1)	117.5(11)
C(5)–C(12)–P(1)	118.1(11)
N(31)–C(6)–C(23)	128.7(12)
N(31)–C(6)–C(61)	115.1(13)
C(23)–C(6)–C(61)	116.1(12)
C(6)–N(31)–N(3)	118.4(11)
C(12)–C(5)–N(3)	119.9(12)
C(12)–C(5)–C(51)	117.4(12)
N(3)–C(5)–C(51)	122.5(11)
C(6)–C(23)–P(2)	112.6(10)
C(4)–C(41A)–C(42A)	122(2)
O(42)–C(41)–O(43)	121(2)
O(42)–C(41)–C(4)	127(2)
O(43)–C(41)–C(4)	112.3(14)
C(41)–O(43)–C(45)	117(2)
C(42A)–O(44A)–C(45A)	114(2)
O(43A)–C(42A)–O(44A)	121(2)
O(43A)–C(42A)–C(41A)	127(2)
O(44A)–C(42A)–C(41A)	112(2)

In order to get further information on the process that converts complex **1** into complex **2**, as well as on the structural characteristics of the intermediate species, we carried out extended Hückel MO calculations [10] using several model complexes.

In a first approach we tried to understand the electronic and steric factors that control the structural trends of the alkyne moiety.

The structure of complex **2** obtained by X-rays shows that the vinyl ligand is almost perpendicular to the square-planar coordination plane, while in most of the alkyne ligands the C–C bond is coplanar with all the other atoms in the coordination sphere. In order to elucidate this aspect [Pd{$C_2(CO_2Me)_2$}$(PH_3)_2$] [11] was used as a model to study the bonding of the coplanar alkyne ligand. Fig. 4 shows an FMO diagram depicting the interaction between the $Pd(PH_3)_2$ and {$C_2(CO_2Me)_2$} fragments.

The five occupied orbitals of the metallic fragment are essentially *xz*, x^2-y^2, *yz*, *xy* and z^2, while the three occupied orbitals of the alkyne ligand are the C–C σ bond, the C–C out-of-plane π-bond and the C–C in-plane π-bond. Although these three orbitals have appropriate symmetry to interact with z^2, *yz* and z^2 metal orbitals, respectively, the result for each of them is a repulsive four-electron interaction, which does not contribute to the bonding. The only orbital with a positive overlap population (0.2 electrons) corresponds to a π donation from the *xz* orbital to the in-plane C–C π* orbital of the alkyne ligand.

Neverthless, the second higher occupied molecular orbital (SHOMO) that results from one of the four electron interactions is responsible for the in-plane conformational preference, as can be seen from the Walsh diagram corresponding to a 90° rotation of the alkyne ligand (Fig. 5(a)).

The results displayed on Fig. 5(a) allow us to conclude that the energy barrier for the rotation of the alkyne is about 0.8 eV, which makes the rotation almost impossible. In fact, from Fig. 6, which depicts the SHOMO orbital (interaction with the out-of-plane C–C π-bond) for the in-plane (a), or perpendicular-to-plane (b) conformations of the alkyne ligand, we can conclude that the orbital in the perpendicular configuration (b) has *anti*-bonding character in what concerns the phosphine ligand, this being in agreement with the high energy for the rotation of the alkyne ligand.

In contrast, for the LUMO orbital (interaction with in-plane π* orbital), the perpendicular conformation (Fig. 7(b)) is more stable due to the Pd–P *anti*-bonding character in the in-plane conformation (Fig. 7(a)).

By electrochemical reduction, one electron is placed at the LUMO, which has a P–Pd–P *anti*-bonding character for the in-plane conformation (see Fig. 4), thus reducing the energy barrier for the rotation of the alkyne ligand. If we consider that the electron trans-

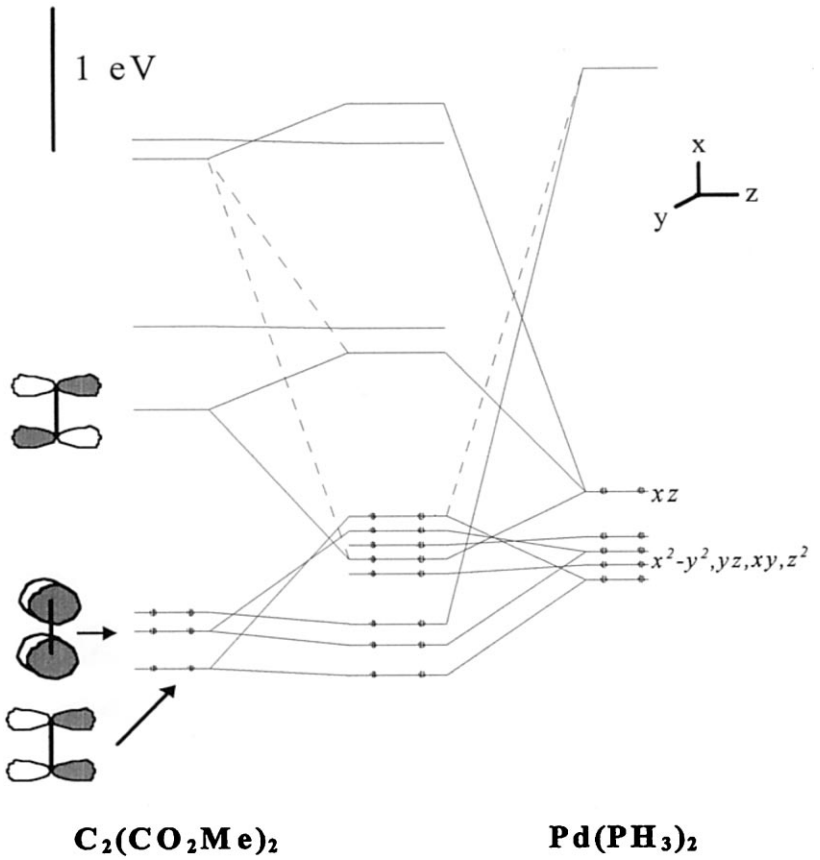

Fig. 4. FMO interaction diagram for the [Pd{$C_2(CO_2Me)_2$}$(PH_3)_2$] complex.

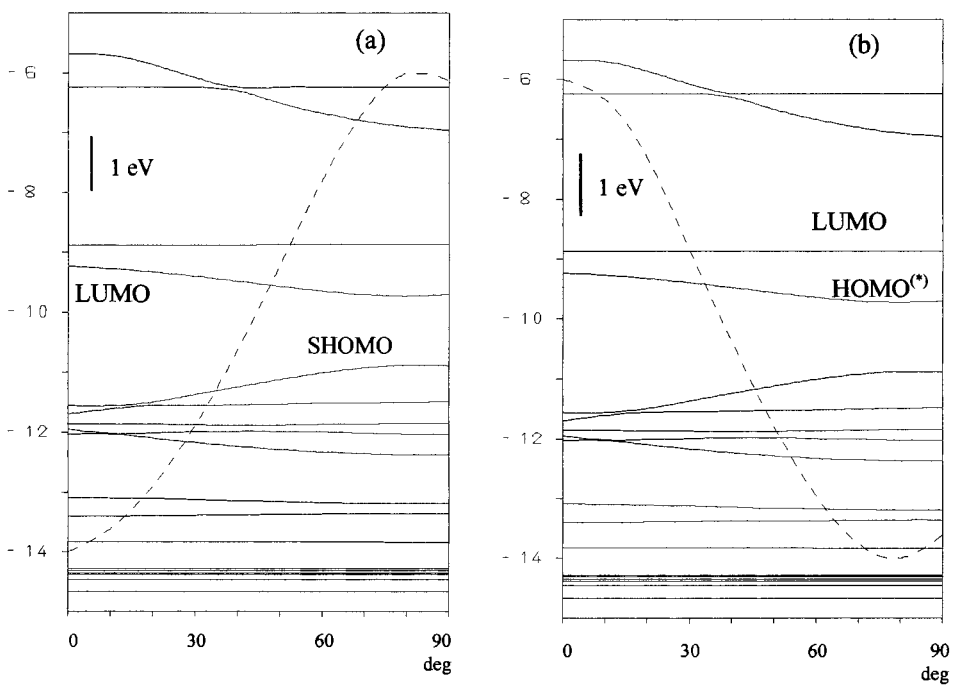

Fig. 5. Walsh diagram for the 90° rotation of the alkyne (a) or the vinyl-type ligand (b). The dashed line corresponds to the total energy. At the x-axis, 0° corresponds to the in-plane and 90° to perpendicular to the in-plane conformation. (*) Corresponds to the former LUMO for the in-plane conformation (a).

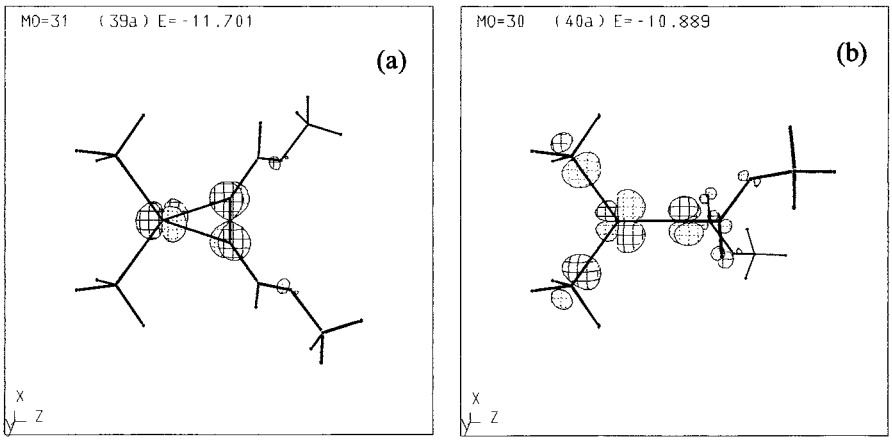

Fig. 6. SHOMO orbital for the two limiting conformations of the alkyne ligand.

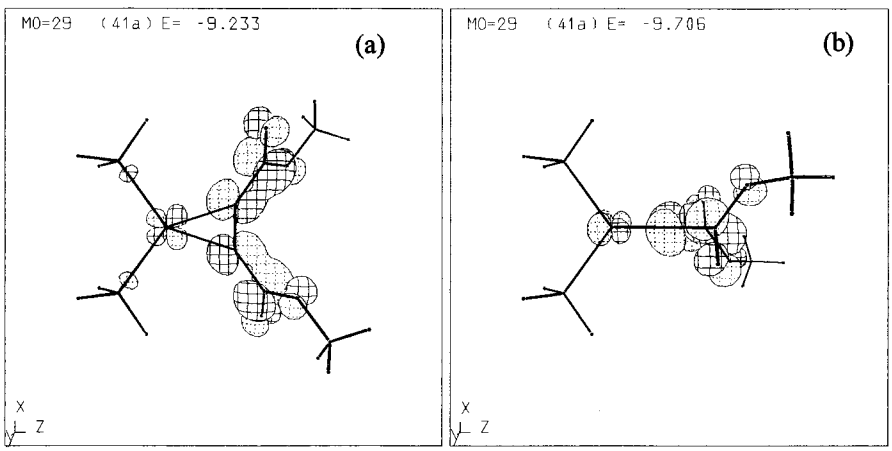

Fig. 7. LUMO orbital for the in-plane (a) or perpendicular-to-plane (b) conformations of the alkyne ligand.

ferred to the LUMO decreases the metal–ligand bond order to 0.5, then the transfer of one electron from the HOMO to the LUMO (more localised at the organic ligand) will allow the LUMO to fill up, thus corresponding to the oxidation of the metal, in the process that converts the organic fragment into a vinyl-type ligand. The electron transfer from the HOMO, with a significant metal character, induced by the geometry change, from in-plane to perpendicular-to-plane, will then formally oxidise the metal from Pd(0) to Pd(I) as discussed before.

The Walsh diagram (Fig. 5(b)) allows us to conclude that the perpendicular conformation will become favourable by about 0.8 eV.

At this stage the ligand can reorganise to improve the overlap population with the z^2 orbital as shown in Fig. 8.

The one-electron-oxidised metal has now a strong tendency to open the P–Pd–P angle, provided that one electron will be removed from the still half-filled orbital (see above), as shown in the Walsh diagram depicted in Fig. 9 (P–Pd–P $\cong$ 170°). This will give the phosphines an almost *trans* geometry.

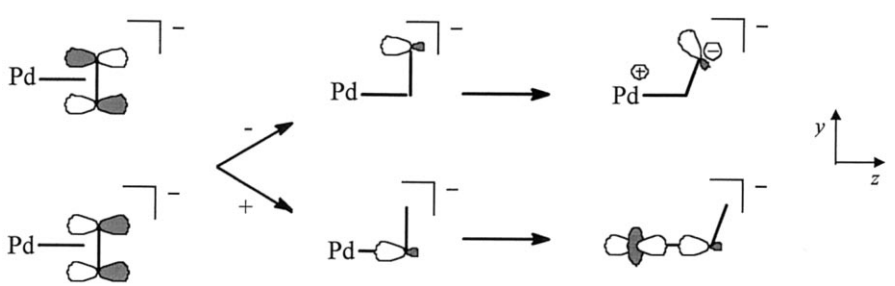

Fig. 8. Scheme of the mixing of the π and π* orbitals to produce a vinyl ligand by shifting the alkyne ligand in the *y*-direction.

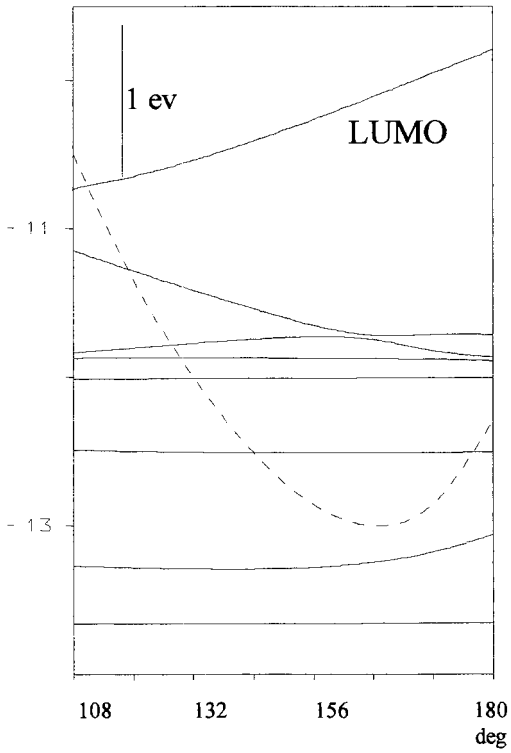

Fig. 9. Walsh diagram for the vinyl complex displaying the effect of the opening of the P–Pd–P angle, from *cis* to *trans*.

In complex **1** the widening of the P–Pd–P angle will favour the approach of the nitrogen atom of the azine moiety to palladium and, thus, bond formation. Moreover, the molecule will then have a convenient geometry to promote proton abstraction, from the five-membered ring CH_2 group of the azine diphosphine ligand, by the anionic vinyl-type ligand.

The migration of such a proton from the diphosphine ligand will complete the alkyne to vinyl conversion and the azine to *ene*-hydrazone transformation.

At this stage electron transfer to a suitable oxidising agent such as the solvent or adventitious oxygen will afford the final neutral complex.

3. Experimental

All the manipulations were done under nitrogen or argon. The solvents were purchased from LabScan, pre-dried and distilled immediately before use. $[Pd_2(DBA)_3]$ [12] and $PPh_2CH_2C(Bu^t)$=NN=$C(Bu^t)$-CH_2PPh_2 [1] were synthesised according to reported procedures. Dimethylacetylene dicarboxylate (DBA) was used as received from Aldrich.

$^{31}P\{H\}$-NMR spectra were recorded on a Varian Unity 300 MHz instrument at 121.4 Hz and chemical shifts were measured relatively to H_3PO_4. ^1H-NMR, ^{13}C-NMR and COSY correlation were made in a Varian Unity 500 instrument at 499.9 or 125.7 Hz, respectively, using hexamethyldisilane as an internal standard. IR spectra were recorded in KBr pellets on a Perkin–Elmer 683 infrared spectrophotometer. FAB mass spectra was recorded in 1,4 butanediol matrix using a Carlo Erba Instruments Auto/HRGC/Trio 2000 MS spectrometer at room temperature.

3.1. Synthesis of $[Pd\{PPh_2CH_2C(Bu^t)=NN=C(Bu^t)CH_2PPh_2\}\{C(CO_2Me)C\equiv C(CO_2Me)\}$ (1)

Azine diphosphine ($PPh_2CH_2C(Bu^t)$=NN=$C(Bu^t)$-CH_2PPh_2) (316 mg, 0.56 mmol) and tris(dibenzylideneacetone)dipalladium (257 mg, 0.28 mmol) in toluene (20 cm^3) were mixed and stirred overnight at room temperature, then DBA (77 mg, 0.54 mmol) in toluene (1 cm^3) was added and the mixture was stirred again overnight. The solution was concentrated to ca. 5 cm^3 and upon addition of isooctane (5 cm^3), yellow crystals precipitated (after several days), which were identified as dibenzylideneacetone. Off-white crystals of the product separated from the solution after filtration, yield 212 mg (48%). The product was recrystallised from benzene–pentane.

NMR data for **1**: δ_P (C_6D_6, ref. to 85% H_3PO_4) 36.0; δ_H (C_6D_6, hexamethyldisilane) 0.67 [9H, s], 2.77 [1H, dd, $^2J(HH) = 12.6$ Hz, $^2J(PH) = 12.6$ Hz], 2.80 [3H, s], 4.45 [1H, dd, $^2J(HH) = 12.6$ Hz, $^2J(PH) = 12.6$ Hz]; δ_C (C_6D_6, hexamethyldisilane) 28.8 [s, $C(CH_3)_3$], 33.9 [d, CH_2, $^1J(PC) = 6.5$ Hz], 38.9 [s, $C(CH_3)_3$], 51.7 [s, OCH_3], 113.3 [dd, $C\equiv$, $^2J(PC) = 7.2$ Hz, $^2J(PC) = 28$ Hz], 163.8 [t, C=N, $|^2J(PC) + {}^4J(PC)| = 12.7$ Hz], 170.6 [s, C=O].

3.2. Electrochemical studies

The electrochemical studies were done in an EG&G PAR 173 potentiostat/galvanostat and an EG&G PARC 175 universal programmer, using a 0.2 M $[NBu_4][BF_4]$–THF or CH_3CN solution. THF was predried over sodium wire and distilled immediately before use. All the manipulations were done under an inert atmosphere. Pt wire and Pt gauze were used as working electrodes for cyclic voltammetry and controlled potential electrolysis, respectively. The potential values are quoted versus SCE and were measured using $[Fe(\eta^5\text{-}C_5H_5)_2]^{0/+}$ ($E = 0.54$ V, vs. SCE) as an internal standard.

3.3. Electrosynthesis of *trans*-$[Pd\{PPh_2CH=C(Bu^t)NN=C(Bu^t)CH_2PPh_2\}\{C(CO_2Me)=CH(CO_2Me)\}]$ (1)

Complex **1** (180 mg, 0.22 mmol) was dissolved in the electrolyte solution (15 cm^3) contained in the cell. The

potential was set at a value ca. 60 mV more negative than that of the peak of the cathodic wave. When the current intensity dropped to a constant value, the electrolysis was stopped and the solution, which changed from pale yellow to orange, was transferred to a Schlenk tube and the solvent evaporated under vacuum. Recrystallisation from *n*-pentane–methanol allowed the separation of the electrolyte ($[NBu_4][BF_4]$, 3.0 mmol) and afforded (55 mg) of complex **2** (31% yield).

4. Crystal-structure determination of complexes 1 and 2

4.1. Crystal data for complex *1*

$C_{42}H_{48}N_2O_4P_2Pd.C_6H_6$, $M = 969.4$, crystallises at the monoclinic space group $C2/C$ with $a = 10.940(1)$, $b = 22.086(1)$, $c = 19.042(2)$ Å, $\beta = 92.692(9)°$, $U = 4596$ Å^3, $D_{calc.} = 1.29$ g cm^{-3}, $T = 293$ K, $Z = 4$, μ(Mo–K$_\alpha$) = 4.5 cm^{-1}. The unit cell and orientation matrix were obtained by least-squares refinement of 25 centred reflections with $15 < \theta < 16°$ using CAD4 centring routines. 4376 reflections, from which 4042 independent ($R_{int} = 0.014$), were collected through a CAD4 diffractometer using variable scan speed to assure constant statistical precision. Three standard reflections were measured every hour, which were used to check the stability of the crystal and of the experimental conditions. The orientation of the crystal was checked by measuring five standards every 100 reflections.

The position of the Pd atom was obtained by a tridimensional Patterson synthesis and it was found to be located at the special position 2. All the other non-hydrogen atoms were located in subsequent different Fourier maps and refined with anisotropic thermal motion parameters. The hydrogen atoms were inserted in calculated positions and refined isotropically with fixed distances to the parent carbon atom. The benzene molecule was refined isotropically. Final refinement converged at $R_1 = 0.048$ ($R_1 = 0.036$ $I > 3\sigma(I)$).

4.2. Crystal data for complex *2*

$C_{42}H_{48}N_2O_4P_2Pd$, $M = 891.4$ crystallises at the triclinic space group $P\bar{1}$ with $a = 11.302(1)$ Å, $b = 12.528(1)$ Å, $c = 16.028(2)$ Å, $\alpha = 107.64(2)°$, $b = 92.27(1)°$ and $\gamma = 111.79(2)°$, $U = 1978$ Å^3, $Z = 2$, $D_{calc.} = 1.37$ g cm^{-3}, $\mu = (Mo–K_\alpha) = 5.2$ cm^{-1}. The unit cell and orientation matrix were obtained by least-squares refinement of 25 centred reflections with $15 < \theta < 18°$. 7225 reflections with $1.5 < \theta < 25°$ were collected by the $\omega - 2\theta$ scan mode, in an Enraf–Nonius CAD4 diffractometer using graphite monochromated radiation. Three standard reflections were monitored during data collection but no decay or instrumental instability was detected (the loss of intensity is less then 0.02% h^{-1}). Using the CAD4 software data were corrected for Lorentz and polarisation effects and empirically for absorption (minimum transmission factor 83.5%, average transmission factor 94.9%). 6947 unique reflections with $F \geq 0$ were used in structure solution and refinement of 460 parameters. The position of the Pd atom was obtained by a tridimensional Patterson synthesis. All the other non-hydrogen atoms were located in subsequent difference Fourier maps and refined with anisotropic thermal motion parameters. The hydrogen atoms were inserted in calculated positions and refined isotropically with fixed distances to the parent carbon atom. Final refinement converged at $R_1 = 0.106$ ($I > 3\sigma(I)$). The largest-peak in the final difference Fourier synthesis was 1.2 e Å^{-3} and was located at 1.3 Å of the Pd atom. The molecular structure is shown in Fig. 4. Selected crystallographic and other relevant data, lists of observed and calculated structure factors, tables of atomic coordinates, anisotropic thermal parameters, hydrogen atomic coordinates, bond lengths and angles and inter- and intra-molecular contact distances are available as supplementary material. The structure solution and refinement were done with SHELX-86 [13] and SHELX-93 [14], respectively and the illustrations were drawn with ORTEP [15]. The atomic scattering factors and anomalous scattering terms were taken from the international table of X-ray crystallography [16].

5. Supplementary material

Tables with X-ray data for complexes **1** and **2** are available on request from the author.

Acknowledgements

This work was partially supported by the Junta Nacional de Investigação Científica e Tecnológica (JNICT), the PRAXIS XXI programme, the Fundação Calouste Gulbenkian (through a travel grant), the Cultural Protocol between Portugal and the Czech Republic, the Instituto de Cooperação Científica e Tecnológica Internacional (ICCTI)/Academy of Sciences of the Czech Republic (ASCR) Protocol and the Grant Agency of the Czech Republic (no. 203/97/1157).

References

[1] S.D. Perera, B.L. Shaw, M. Thornton-Pett, J. Chem. Soc. Dalton Trans. (1992) 1469.
[2] S.D. Perera, B.L. Shaw, M. Thornton-Pett, J. Chem. Soc. Dalton Trans. (1993) 3653.
[3] S.D. Perera, B.L. Shaw, M. Thornton-Pett, J. Chem. Soc. Dalton Trans. (1994) 3311.

[4] P.A. Cooke, S.D. Perera, B.L. Shaw, M. Thornton-Pett, J.D. Vessey, Chem. Soc. Dalton Trans. (1997) 435 and references therein.
[5] A.G. Orpen, L. Brammer, F.H. Allen, O. Kennard, D.G. Watson, R. Taylor, J. Chem. Soc. Dalton Trans. (1989) S1.
[6] F.H. Allen, J.E. Davies, J.J. Galloy, O. Johnson, O. Kennard, C.F. Macrae, E.M. Mitchell, G.F. Mitchel, M.J. Schmith, D.G.J. Watson, Chem. Inf. Comput. Sci. 31 (1991) 187.
[7] G. Erker, U. Korek, J. Petrersen, J. Organomet. Chem. 355 (1988) 121.
[8] A.S. Viana, M.F.N.N. Carvalho, A.J.L. Pombeiro, R. Herrmann, Inorg. Chim. Acta 258 (1997) 201.
[9] S.D. Perera, B.L. Shaw, J. Chem. Soc. Dalton Trans. (1995) 3861 and references therein.
[10] C. Mealli, D.M. Proserpio, J. Chem. Educ. 67 (1990) 399.
[11] J.A. McGinnety, J. Chem. Soc. Dalton Trans. (1974) 1038.
[12] T. Ukai, H. Kawazura, Y. Ishii, J.J. Bonnet, J.A. Ibers, J. Organomet. Chem. 65 (1974) 253.
[13] G.M. Sheldrick, SHELX-86, in: G.M. Sheldrick, Krüger, R. Goddard (Eds.), Crystallographic Computing 3, Oxford University, London, 1985, p. 175.
[14] G.M. Sheldrick, SHELX-93, A Computer Program for Crystal Structure Determination, University of Göttingen, Germany, 1993.
[15] C.K. Johnson, ORTEP-II, Report ORNL-5138, Oak Ridge National Laboratory, Park Ridge TN, 1976.
[16] International Tables for X-ray Crystallography, vol. IV, Kynoch, Birmingham, 1974.